Supporting Information

Asymmetric deep-blue tetrafluorobenzene-bridged fluorophores with hybridized local and charge-transfer characteristics for efficient OLEDs with low efficiency roll-off

Shengnan Wang,[a] Haoyuan Qi,[a] Hao Huang,[a] Jie Li,[a] Yuchao Liu,[a] Shanfeng Xue,[a] Shian Ying,[a]*

Changsheng Shi,[b] *and Shouke Yan*[a, b]*

[a] Key Laboratory of Rubber-Plastics, Ministry of Education, Qingdao University of Science & Technology,

Qingdao 266042, P. R. China.

[b] School of Physics and Astronomy, Yunnan University, Kunming 650091, P. R. China.

[c] State Key Laboratory of Chemical Resource Engineering, College of Materials Science and Engineering,

Beijing University of Chemical Technology, Beijing 100029, P. R. China.

E-mail: shian0610@126.com (S. Ying); csshi@ynu.edu.cn (C. Shi); skyan@mail.buct.edu.cn (S. Yan)

1. Experimental Section

1.1 General information

The raw materials and reagents were used after purchase without further purification. ^{1}H and ^{13}C nuclear magnetic resonance (NMR) spectra were performed on a Bruker AVAN CE NEO 400 spectrometer with tetramethyl silane (TMS) as the internal standard in chloroform-d (CDCl$_3$) solution. High-resolution mass spectra (MS) of target materials were measured by using a high-resolution quadrupole time of flight tandem mass spectrometer (TOF-MS) operating in MALDI-TOF mode. The elemental analysis were carried out with Perkin–Elmer 2400. Ultraviolet-visible (UV-vis) absorption and photoluminescence (PL) spectra in dilute solutions were measured by HITACHI U-4100 and F-4600 fluorescence spectrofluorometers. Transient PL spectra were measured using a FLS1000 transient fluorescence spectrometer. Photoluminescence quantum yields (PLQYs) of compounds in solution and film were tested employing the integration sphere setup (Hamamatsu C11347-11) equipped with a xenon high-pressure lamp. Thermogravimetric analysis (TGA) curves of materials were performed using a Netzsch (209F1) thermogravimetric analyzer under a nitrogen atmosphere (50 mL min^{-1}) at a heating rate of 10 °C min^{-1}. Differential scanning calorimetry (DSC) curves of target compounds were recorded by a Netzsch DSC (204F1) instrument at a heating (or cooling) rate of 10 °C min^{-1}. Cyclic voltammetry (CV) was measured on a CHI660E electrochemical workstation in a conventional three-electrode system including a glass carbon working electrode, a platinum wire auxiliary electrode, and an Ag/Ag$^+$ standard reference electrode, where tetrabutylammonium hexafluorophosphate (Bu4NPF6, 0.1 M) in anhydrous dichloromethane (DCM) acted as the supporting electrolyte and ferrocene served as the standard reference. The HOMO (E$_{HOMO}$) and LUMO (E$_{LUMO}$) energy levels can be calculated by the following formula:

$$E_{HOMO} = -(E_{ox} - E_{1/2}^+ + 4.80) \text{ eV} \quad （1）$$

$$E_{LUMO} = (E_{HOMO} + E_g) \text{ eV} \qquad （2）$$

Here, E_{ox} is the oxidation onset potentials. $E_{1/2}^+$ is half wave potentials of Fc^+ /Fc^-vs Ag/Ag^+ acquired from the CV curves of oxidation and reduction. E_g was the optical bandgap evaluated from the onset of absorption spectra.

1.2 Device Preparation

Patterned indium-tin-oxide (ITO) glasses underwent ultrasonic cleaning in detergents and deionized water, followed by drying at 120 °C for a duration of 30 minutes. Subsequently, the ITO-substrates were treated with oxygen plasma and then carefully transferred to the vacuum deposition system. The devices were crafted in a high-vacuum environment, maintaining a pressure below 2×10^{-4} Pa. Evaporation rates were precisely monitored using a frequency counter and calibrated with a Dektak 6 M profiler from Veeco. Organic materials, lithium fluoride (LiF), and aluminum (Al) were thermally evaporated through a shadow mask at controlled rates of 1-1.5, 0.2, and 5-10 Å s^{-1} respectively. The emitting area of the devices, defined by the overlap between ITO and Al electrodes, measured 3×3 mm^2. To assess device performance, we recorded the current density, luminance, and voltage characteristics using a Keithley 2450 source meter and an LS160 luminance meter. Additionally, EL spectra were captured with an optical analyzer, the FlAME-S-VIS-NIR photometer. Assuming the light emitted by the OLEDs follows a Lambertian distribution, the external quantum efficiencies (EQEs) are estimated based on the EL spectra, luminance, and current density measurements.

1.3 Theoretical calculation

All density functional theory (DFT) and time-dependent DFT (TD-DFT) calculations for the target materials were conducted utilizing the Gaussian 09 software package. The optimized ground-state geometries, energy levels, and frontier molecular orbital (FMO) distributions were determined using the B3LYP/6-31G(d, p) method within the DFT framework. Furthermore, based on the TD-DFT approach and employing the same B3LYP/6-31G(d, p)

method, we calculated the optimized excited-state geometries, natural transition orbitals (NTOs), singlet and triplet state energies, as well as oscillator strengths. Spin-orbit coupling (SOC) matrix elements were calculated by TD-DFT and the ORCA 4.1.1 package at B3LYP/6-31G(d, p).

1.4 Synthesis and characterization of target materials
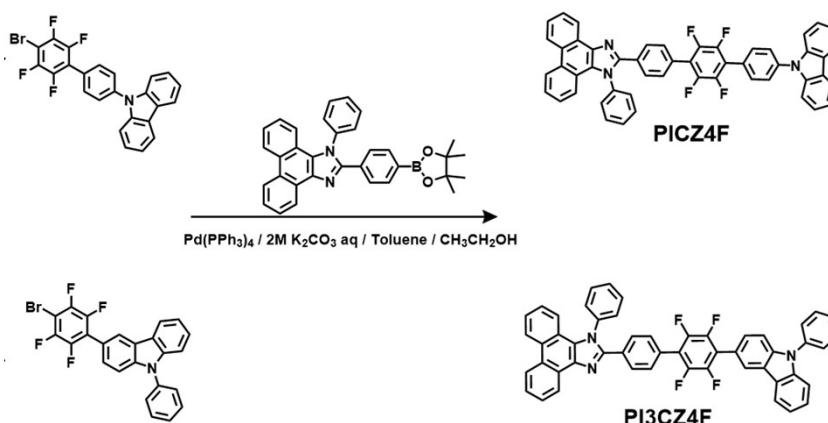
Scheme S1. Synthetic Routes to **PICZ4F** and **PI3CZ4F**.

*Synthesis of 2-(4''-(9H-carbazol-9-yl)-2',3',5',6'-tetrafluoro-[1,1':4',1''-terphenyl]-4-yl)-1-phenyl-1H-phenanthro[9,10-d]imidazole (**PICZ4F**)*

In N_2 atmosphere, 9-(4'-bromo-2',3',5',6'-tetrafluoro-[1,1'-biphenyl]-4-yl)-9*H*-carbazole (1.35 g, 2.87 mmol), 1-phenyl-2-(4-(4,4,5,5-tetramethyl-1,3,2-dioxaborolan-2-yl)phenyl)-1*H*-phenanthro[9,10-*d*]imidazole (1.72 g, 3.4 mmol) and tetrakis-triphenylphosphine palladium Pd(PPh$_3$)$_4$ (0.13 g, 0.11 mmol) were added into the two-neck round-bottom flask. 2M potassium carbonate solution (10 mL), CH$_3$CH$_2$OH (10 mL) and toluene (30 mL) were injected into flask using syringes. After refluxed for 24 h, the reaction mixture was cooled down to room temperature. Then the mixture was extracted three times using dichloromethane, and the organic phase was dried over anhydrous magnesium sulfate. After filtration and evaporation, the crude product was purified by silica-gel column chromatography using

dichloromethane/ petroleum (1/10, v/v) as the solvent, Finally, the product was prepared by recrystallization using the mixed solvent of dichloromethane and ethanol to give a white solid (Yield: 2.11 g, 81.78%). ^{1}H NMR (400 MHz, CDCl$_3$) δ 8.79 (d, J = 8.4 Hz, 1H), 8.72 (d, J = 8.3 Hz, 1H), 8.30 (s, 1H), 8.18 (d, J = 7.7 Hz, 1H), 7.78 (t, J = 7.5 Hz, 3H), 7.73 – 7.50 (m, 16H), 7.50 – 7.45 (m, 1H), 7.45 – 7.40 (m, 1H), 7.37 – 7.27 (m, 2H), 7.20 (d, J = 8.2 Hz, 1H); ^{13}C NMR (101 MHz, CDCl$_3$) δ 149.90, 143.03, 141.38, 141.03, 138.64, 137.31, 130.39, 130.18, 130.09, 130.03, 129.45, 129.35, 129.13, 128.41, 128.38, 128.19, 127.85, 127.41, 127.16, 126.54, 126.36, 125.81, 125.10, 124.17, 123.59, 123.16, 123.09, 122.99, 122.86, 122.41, 120.94, 120.49, 120.46, 118.66, 110.08, 109.98. Anal. Calcd. for C51H29F4N3: C, 80.62; H, 3.85; F, 10.00; N, 5.53; Found: C, 80.25; H, 3.832; N, 5.49. TOF-MS(ESI) m/z calcd. for C51H29F4N3: 759.2298; [M+H]$^+$ found: 760.2377.

*Synthesis of 1-phenyl-2-(2',3',5',6'-tetrafluoro-4'-(9-phenyl-9H-carbazol-3-yl)-[1,1'-biphenyl]-4-yl)-1H-phenanthro[9,10-d]imidazole (**PI3CZ4F**)*

The compound PI3CZ4F was synthesized according to the similar procedure as for PICZ4F by using (9-phenyl-9*H*-carbazol-3-yl) boronic acid (2.18 g, 7.59 mmol) instead of (4-(9*H*-carbazol-9-yl)phenyl)boronic acid. And PI3CZ4F was obtained as white solid (Yield: 4.76 g, 82.5%). ^{1}H NMR (400 MHz, CDCl$_3$) δ 8.83 – 8.77 (m, 1H), 8.76 – 8.70 (m, 1H), 8.17 (dt, J = 7.7, 1.0 Hz, 2H), 7.83 – 7.72 (m, 7H), 7.72 – 7.58 (m, 6H), 7.57 – 7.43 (m, 7H), 7.33 (ddd, J = 8.0, 7.1, 1.1 Hz, 2H), 7.30 – 7.25 (m, 2H), 7.21 (dd, J = 8.3, 1.3 Hz, 1H). ^{13}C NMR (101 MHz, CDCl$_3$) δ 140.56, 138.62, 131.78, 130.41, 130.15, 129.43, 129.10, 128.40, 127.00, 126.39, 126.11, 124.19, 123.62, 123.15, 120.94, 120.40, 120.32, 109.82. Anal. Calcd. for C51H29F4N3: C, 80.62; H, 3.85; F, 10.00; N, 5.53; Found: C, 80.40; H, 3.617; N, 5.55. TOF-MS(ESI) m/z calcd. for C51H29F4N3: 759.2298; [M + H]$^+$ found: 760.2374.

1.5 The analysis of dependence of the electric field on hole/electron mobilities

Hole and electron mobilities can be evaluated by a space-charge-limited current (SCLC) method, described by the Mott–Gurney equation, provides a means for analysis (1):

$$J = \frac{9}{8} \varepsilon_0 \varepsilon_r \mu \frac{E^2}{L} \tag{1}$$

In this context, J denotes the current density, ε_0 signifies the vacuum permittivity with a value of 8.85×10^{-14} C V^{-1} cm^{-1}, ε_r represents for the relative dielectric constant, assumed to be 3.0 for the organic semiconductor, μ stands the carrier mobility, E indicates the electric field intensity, and L refers to the thickness of the emitters. Considering the influence of energetic disorder on carrier mobility, the electric field-dependent mobility can be formulated using the Poole–Frenkel equation:

$$\mu = \mu_0 \, e^{-\gamma\sqrt{E}} \tag{2}$$

Here, μ_0 represents the zero-field mobility and γ denotes the Poole–Frenkel factor. Consequently, the SCLC that depends on the electric field can be formulated as follows:

$$J = \frac{9}{8} \varepsilon_0 \varepsilon_r \mu_0 \frac{V^2}{L^3} e^{0.891\gamma\sqrt{\frac{V}{L}}} \tag{3}$$
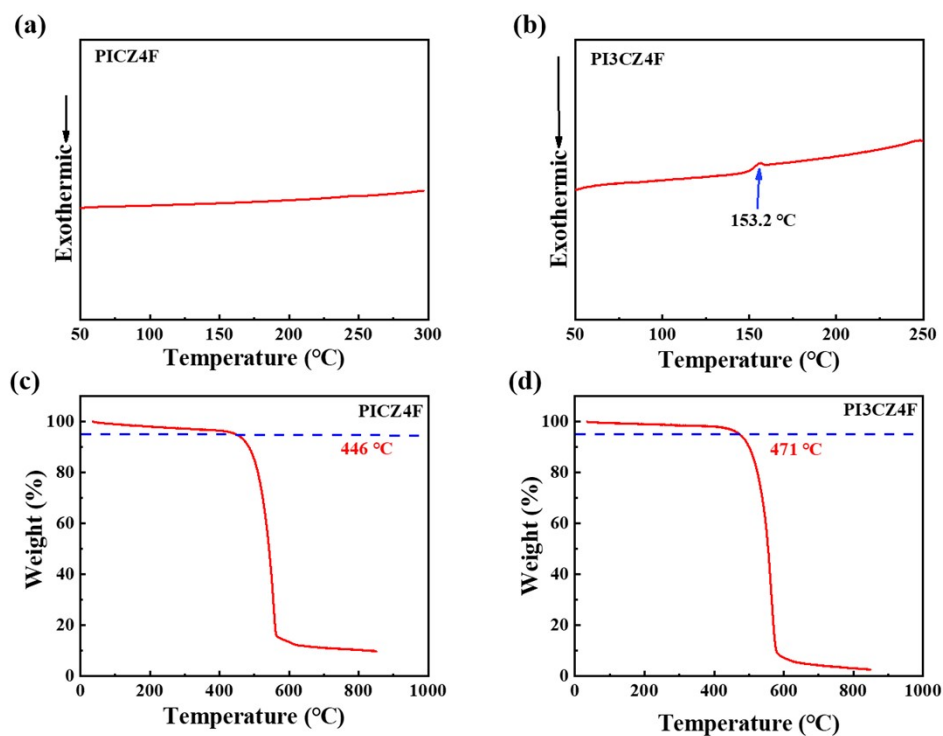
Fig. S1. The DSC curves of **PICZ4F** (a) and **PI3CZ4F** (b). The TGA curves of **PICZ4F**(c) and **PI3CZ4F**(d).
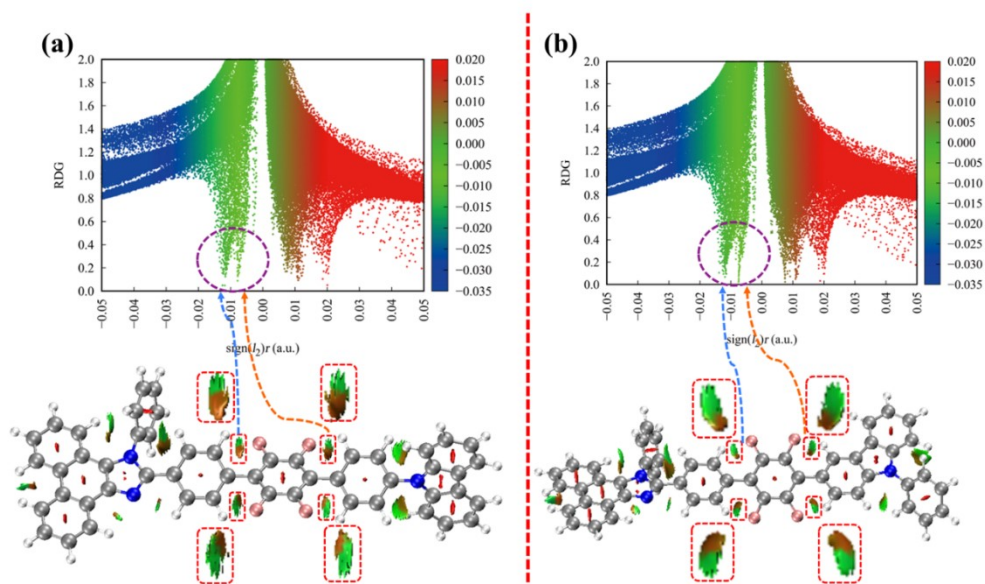

Fig. S2. Optimized S_0 geometries and reduced density gradient (RDG) isosurface map and the functions of RDG and Sign (λ_2) ρ for **PICZ4F** and **PI3CZ4F**.
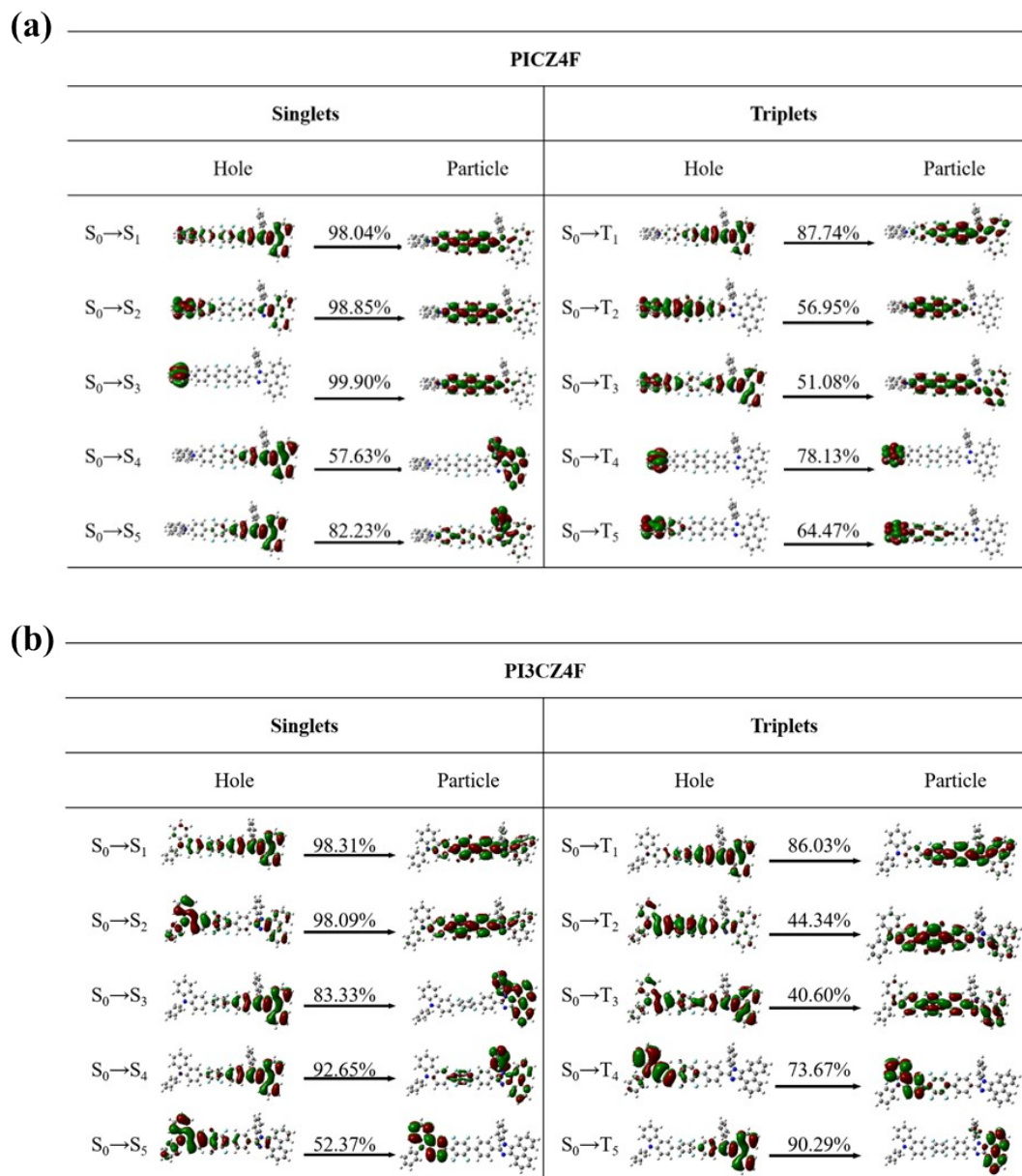
Fig. S3. The natural transition orbitals (NTOs) of the singlet (S_{1-5}) and triplet (T_{1-5}) excited states for **PICZ4F** (a) and **PI3CZ4F** (b) using the Gaussian 09 package at the basis set of B3LYP/ 6-31G(d, p).

Table S1. The singlet and triplet energy levels, and the oscillator strengths of singlet excited states for **PICZ4F**.

S Excited States	[eV]	T Excited States	[eV]	S Oscillator Strength
S_1	3.12	T_1	2.52	1.1738
S_2	3.31	T_2	2.86	0.0169
S_3	3.70	T_3	3.01	0.0000
S_4	3.71	T_4	3.17	0.0013
S_5	3.81	T_5	3.35	0.0208
S_6	3.82	T_6	3.35	0.0880
S_7	3.96	T_7	3.39	0.0332
S_8	4.01	T_8	3.54	0.0648
S_9	4.04	T_9	3.58	0.0081
S_{10}	4.07	T_{10}	3.68	0.2149

Table S2. The singlet and triplet energy levels, and the oscillator strengths of singlet excited states for **PI3CZ4F**.

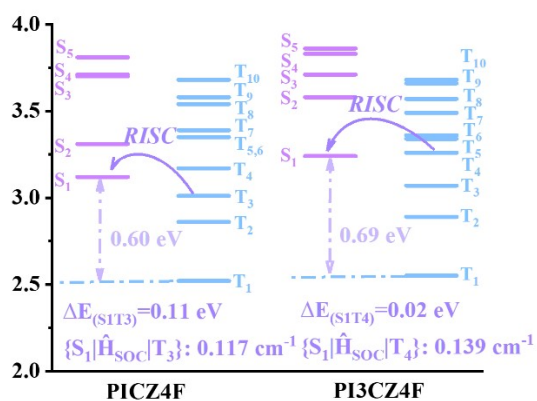| S Excited States	[eV]	T Excited States	[eV]	S Oscillator Strength
S_1	3.24	T_1	2.55	1.3908
S_2	3.58	T_2	2.89	0.1055
S_3	3.71	T_3	3.07	0.0090
S_4	3.83	T_4	3.26	0.0145
S_5	3.86	T_5	3.34	0.0107
S_6	3.90	T_6	3.36	0.0362
S_7	3.98	T_7	3.49	0.0287
S_8	4.04	T_8	3.57	0.1137
S_9	4.11	T_9	3.66	0.0294
S_{10}	4.16	T_{10}	3.68	0.0077

Fig. S4. The plots of energy levels of singlet and triplet states of **PICZ4F** and **PI3CZ4F**.
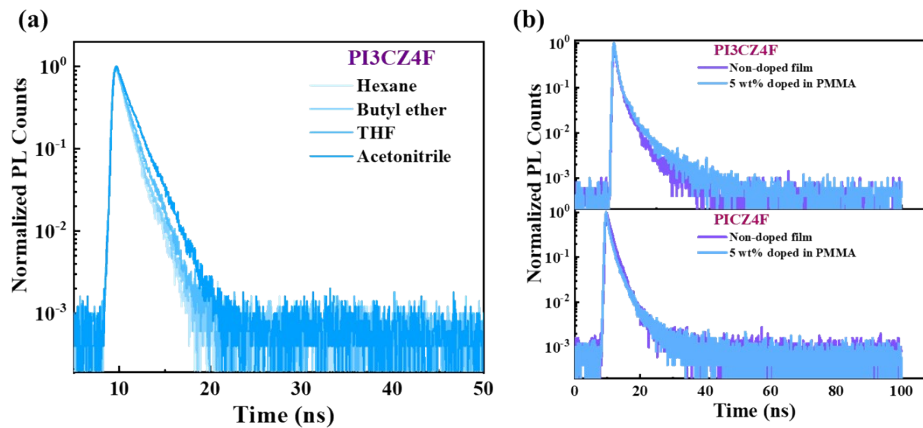
Fig. S5. (a) Transient PL decay spectra of **PI3CZ4F** in the hexane, butyl ether, THF, and acetonitrile solutions (10 μM). (b) Transient PL decay spectra of films for **PICZ4F** and **PI3CZ4F**.

Table S3. Photophysical parameters for **PICZ4F** and **PI3CZ4F** in different solvents and films.

Solutions or films	PICZ4F				PI3CZ4F			
	PLQY[a] [%]	τ[b] [ns]	k_r[c] [$\times 10^8$ s^{-1}]	k_{nr}[d] [$\times 10^8$ s^{-1}]	PLQY[a] [%]	τ[b] [ns]	k_r[c] [$\times 10^8$ s^{-1}]	k_{nr}[d] [$\times 10^8$ s^{-1}]
Hexane	97	1.175	8.26	0.26	97	0.994	9.80	0.30
Butyl ether	98	1.185	8.27	0.16	98	1.052	9.32	0.19
Tetrahydrofuran	99	1.549	6.39	0.06	99	1.180	8.39	0.08
Acetonitrile	99	1.802	5.49	0.06	99	1.467	6.75	0.07
Neat film	80	1.216	6.58	1.64	87	0.971	8.96	1.34
Doped film	97	1.568	6.19	0.19	90	0.905	9.94	1.10

[a] Photoluminescence quantum yield. [b] Fluorescence lifetime. [c] Radiative decay rate. [d] non-radiative decay rate.
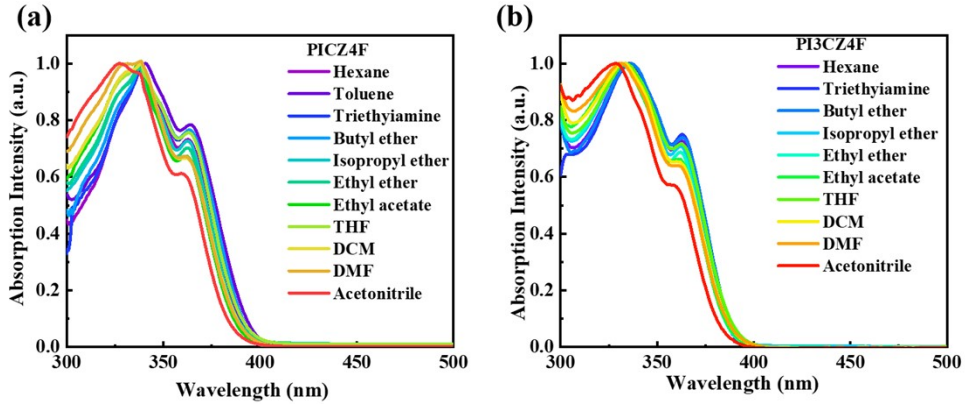
Fig. S6. Absorption spectra of **PICZ4F** (a) and **PI3CZ4F** (b) in different solvents with the concentrations of 10 μM.
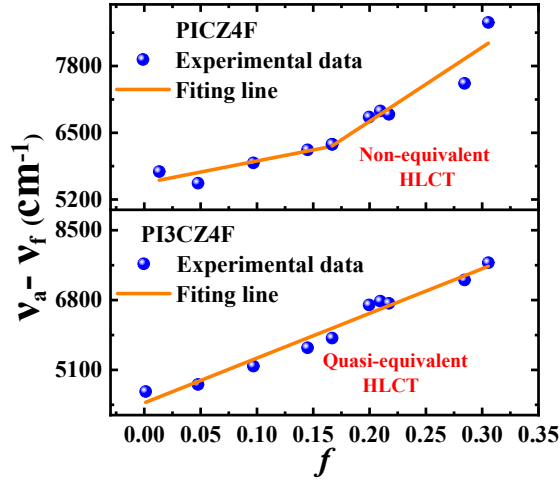

Fig. S7. Lippert–Mataga plots of the Stokes shift (v_a-v_f) against the orientation polarizability f (ε, n).

Detailed Analysis of Lippert-Mataga Calculation

The Lippert-Mataga model is calculated by Equation 1 as below.

$$hc(v_a - v_f) = hc(v_a^0 - v_f^0) + \frac{2(\mu_e - \mu_g)^2}{a_0^3}f(\varepsilon,n) \tag{1}$$

$$f(\varepsilon,n) = \frac{\varepsilon - 1}{2\varepsilon + 1} + \frac{n^2 - 1}{2n^2 + 1} \tag{2}$$

11

$$a_0 = (\frac{3M}{4\pi Nd})^{1/3}$$

(3)

Where h is the Plank constant, c is the light speed in vacuum, μ_g is the ground-state dipole moment; μ_e is the excited-state dipole moment, $f(\varepsilon, n)$ is the orientational polarizability of solvents, a_0 is the Onsager cavity radius, $v_a^0 - v_f^0$ is the Stokes shifts when f is zero, respectively. In Equation 2, ε and n are dielectric constant and refractive index of solvent. In Equation 3, N is Avogadro's number, M is molar mass, and d is density of the solvents, respectively.

Take differential on both sides of the Equation 1, the Equation 4 can be obtained:

$$\mu_e = \mu_g + \{\frac{hca_0^3}{2} \times [\frac{d(v_a - v_f)}{df(\varepsilon, n)}]\}^{1/2}$$

(4)

The μ_g of **PICZ4F** and **PI3CZ4F** (3.97 and 4.09 D, respectively) was estimated with the Gaussian 09 package at the level of RB3LYP/6-31G(d, p), respectively. The value of a_0 can be estimated by the Equation 3. The $\frac{d(v_a - v_f)}{df(\varepsilon, n)}$ can be estimated with the solvatochromic experiment data listed in Table S4 and S5. With the information above, μ_e can be figured out as mentioned in the manuscript.

Table S4. The detailed absorption and emission data of **PICZ4F** in different solvents.

Solvents	ε [a]	n [b]	$f(\varepsilon, n)$ [c]	λ_a [d] [nm]	λ_f [e] [nm]	$v_a - v_f$ [f] [cm⁻¹]
Hexane	1.9	1.375	0.0012	338	406	4955.26
Toluene	2.38	1.494	0.013	339	421	5745.56
Triethylamine	2.42	1.401	0.048	339	417	5517.71
Butyl ether	3.08	1.399	0.096	339	424	5913.62
Isopropyl ether	3.88	1.368	0.145	338	427	6166.60
Ethyl ether	4.34	1.352	0.167	338	429	6275.78
Ethyl acetate	6.02	1.372	0.2	338	439	6806.76
Tetrahydrofuran	7.58	1.407	0.21	339	443	6925.16
Dichloromethane	8.93	1.424	0.217	338	440	6858.53
Dimethylformamide	37	1.427	0.276	338	463	7987.53
Acetone	20.7	1.359	0.284	338	452	7461.91
Acetonitrile	37.5	1.344	0.305	326	454	8648.41

[a] Solvent dielectric constant. [b] Solvent refractive index. [c] Solvent orientation polarizability. [d] Absorption peak wavelength. [e] Emission peak wavelength. [f] Stokes shift.

Table S5. The detailed absorption and emission data of **PI3CZ4F** in different solvents.

Solvents	ε [a]	n [b]	$f(\varepsilon, n)$[c]	λ_a [d] [nm]	λ_f [e] [nm]	$\nu_a - \nu_f$ [f] [cm^{-1}]
Hexane	1.9	1.375	0.0012	336	397	4572.99
Toluene	2.38	1.494	0.013	337	412	5401.75
Triethylamine	2.42	1.401	0.048	337	404	4921.12
Butyl ether	3.08	1.399	0.096	336	407	5191.88
Isopropyl ether	3.88	1.368	0.145	333	410	5639.79
Ethyl ether	4.34	1.352	0.167	333	414	5875.44
Ethyl acetate	6.02	1.372	0.2	331	425	6682.07
Tetrahydrofuran	7.58	1.407	0.21	333	430	6774.22
Dichloromethane	8.93	1.424	0.217	333	429	6720.01
Dimethylformamide	37	1.427	0.276	332	445	7648.57
Acetone	20.7	1.359	0.284	332	438	7289.43
Acetonitrile	37.5	1.344	0.305	328	439	7708.76

[a] Solvent dielectric constant. [b] Solvent refractive index. [c] Solvent orientation polarizability. [d] Absorption peak wavelength. [e] Emission peak wavelength. [f] Stokes shift.
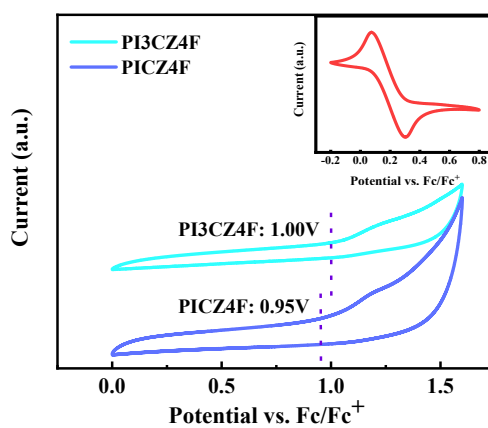
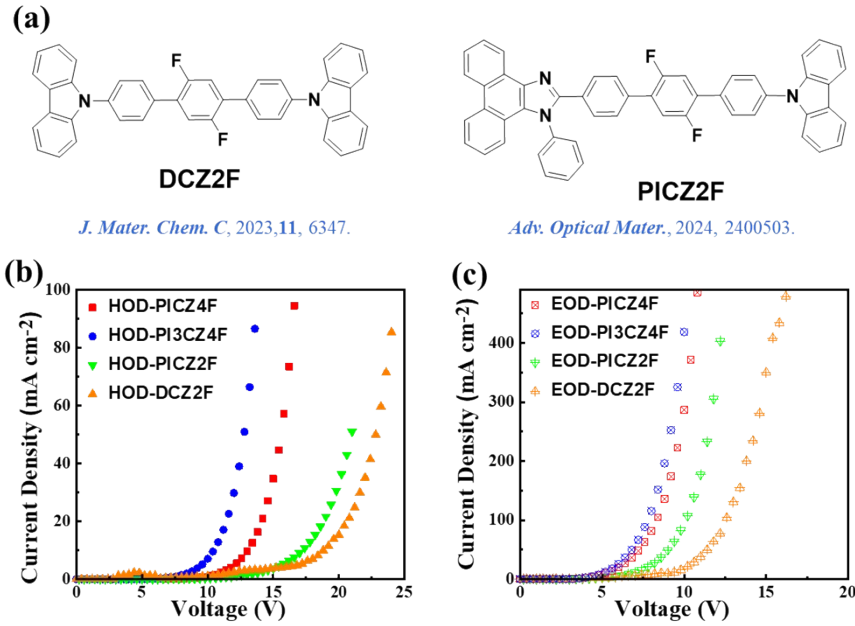**Fig. S8**. Cyclic voltammograms curves of **PICZ4F** and **PI3CZ4F**.

Fig. S9. (a) The molecular structure of DCZ2F and PICZ2F reported in our previous works. (b) The current density-voltage curves of hole-only devices for **PICZ4F**, **PI3CZ4F**, DCZ2F and PICZ2F. (c) The current density-voltage curves of electron-only devices for **PICZ4F**, **PI3CZ4F**, DCZ2F and PICZ2F.
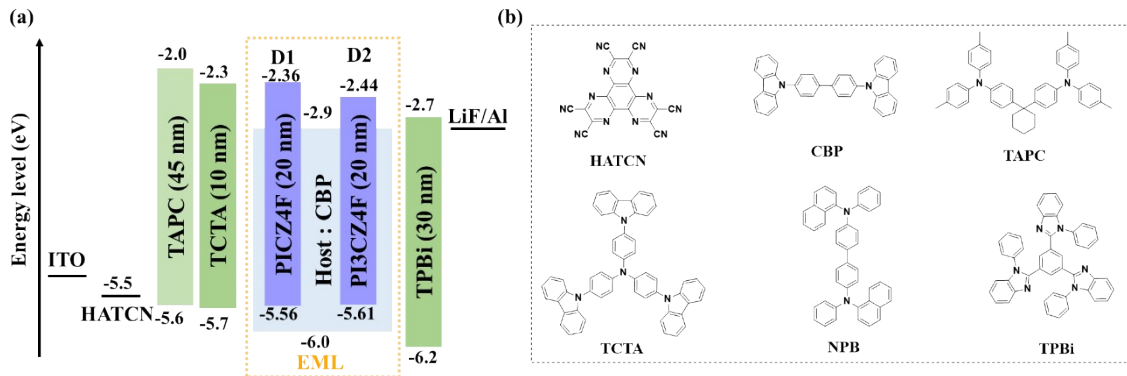

Fig. S10. (a) The energy level diagrams of the functional layer materials. (b) The molecular structure of organic materials used in the OLEDs.
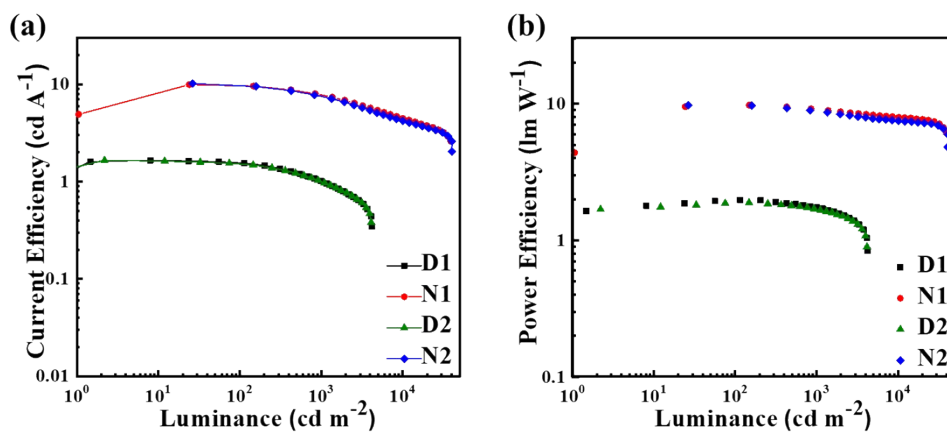
Fig. S11. Power efficiency–luminance characteristics (a) and current efficiency–luminance–efficiency characteristics (b) for the devices. **D1**, **D2**, **N1**, and **N2**.
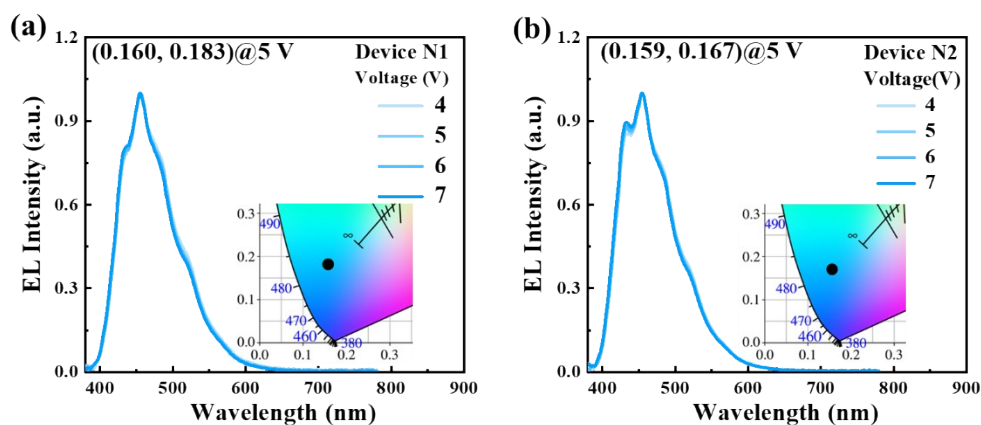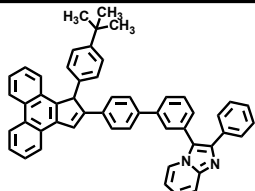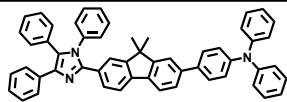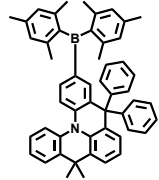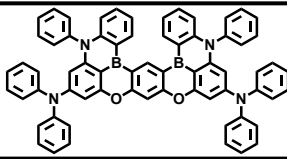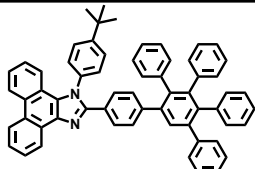

Fig. S12. (a) EL spectra of the device **N1** at the voltages from 4 to 7 V. Inset: CIE chromaticity diagram. (b) EL spectra of the device **N2** at the voltages from 4 to 7 V. Inset: CIE chromaticity diagram.

Table S6. Summary of representative performances of OLEDs with CIEy at the range from 0.040 to 0.055.

Molecular structure	Name	EL peak [nm]	CIE(x, y)	EQE$_{1000}$ [%]	Reference
	PICZ4F	412	(0.159, 0.049)	5.54	This work
	PI3CZ4F	410	(0.159, 0.048)	5.61	This work
	BBPA	432	(0.15, 0.05)	7.25	[1]
	2FPPICZ	425	(0.160, 0.045)	2.5	[2]
	PA-1	-	(0.157, 0.053)	2.3	[3]
	B-O-dpa	442	(0.15, 0.04)	0.8	[4]
	BD1	424	(0.16, 0.05)	3.7	[5]
	2FPPIDPA	433	(0.156, 0.046)	4.36	[6]
	DSiTPI	424	(0.16, 0.05)	5.0	[7]
	PPi-Xid	436	(0.155, 0.052)	3.63	[8]

	PPi-Mid	433	(0.153, 0.052)	3.76	[8]
	TFPBI	441	(0.152, 0.054)	4.80	[9]
	DMCN-B	444	(0.151, 0.045)	2.2	[10]
	BOBO-Z	445	(0.15, 0.04)	3.3	[11]
	TTP-TPI	424	(0.16, 0.05)	3.98	[12]
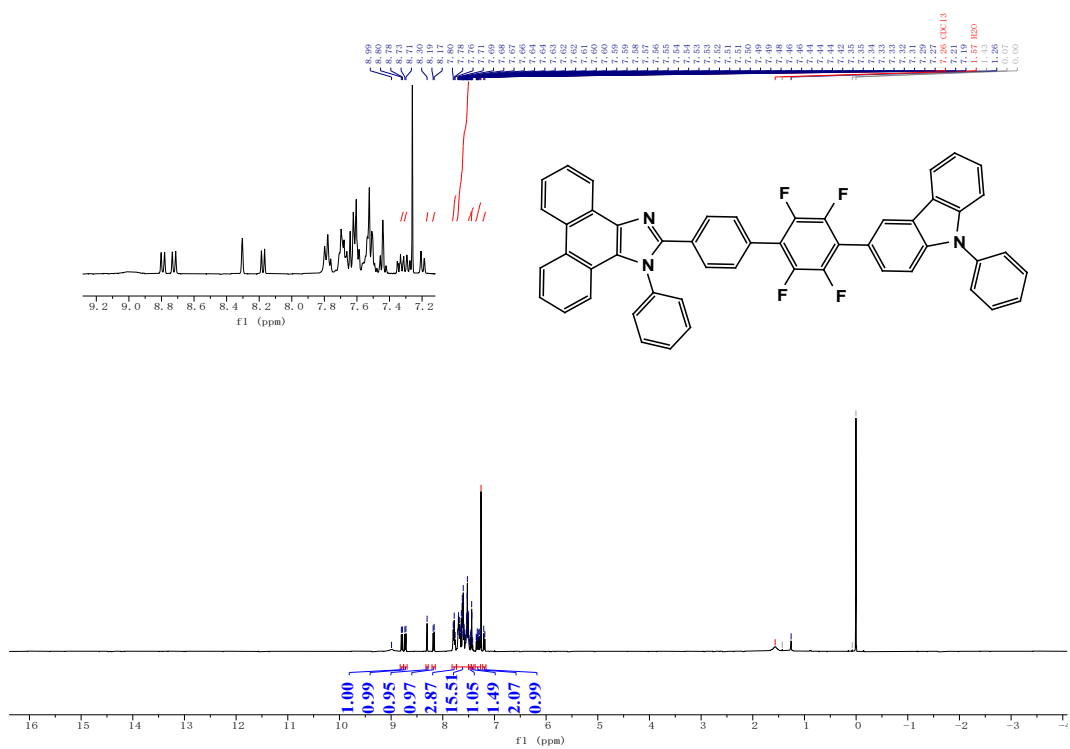
Fig. S13. The ^{1}H NMR spectra of **PI3CZ4F**.

17
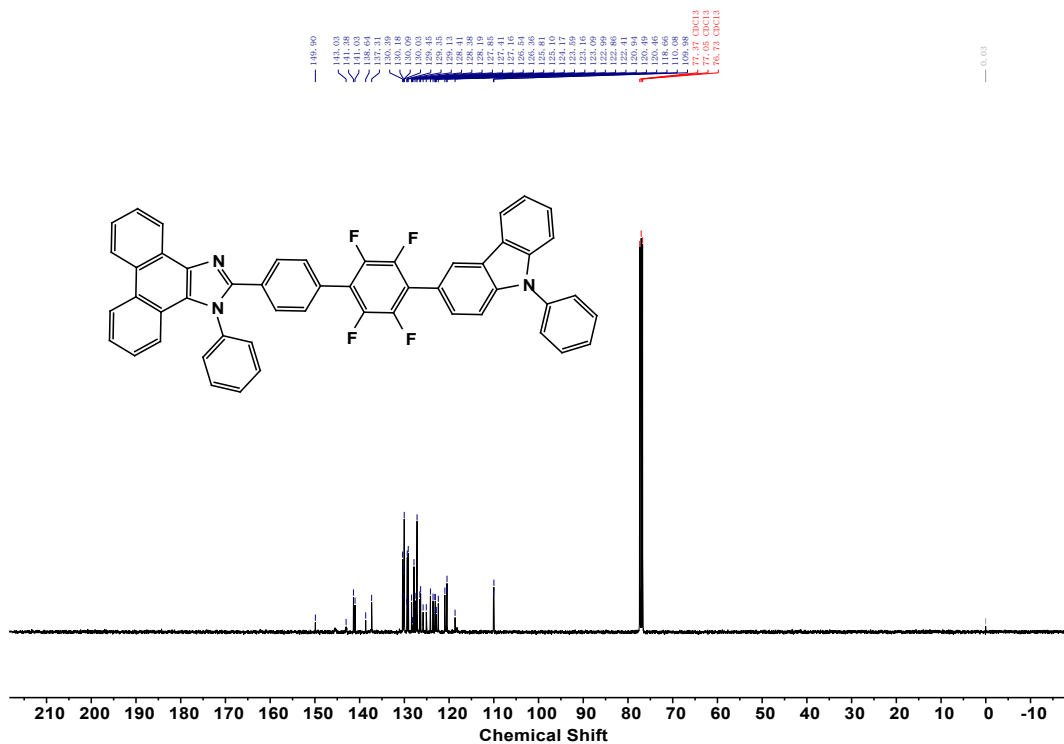
Fig. S14. The ^{13}C NMR spectra of **PI3CZ4F**.

Fig. S15. The HRMS of **PICZ4F**.

Fig. S16. The ¹H NMR spectra of **PICZ4F**.

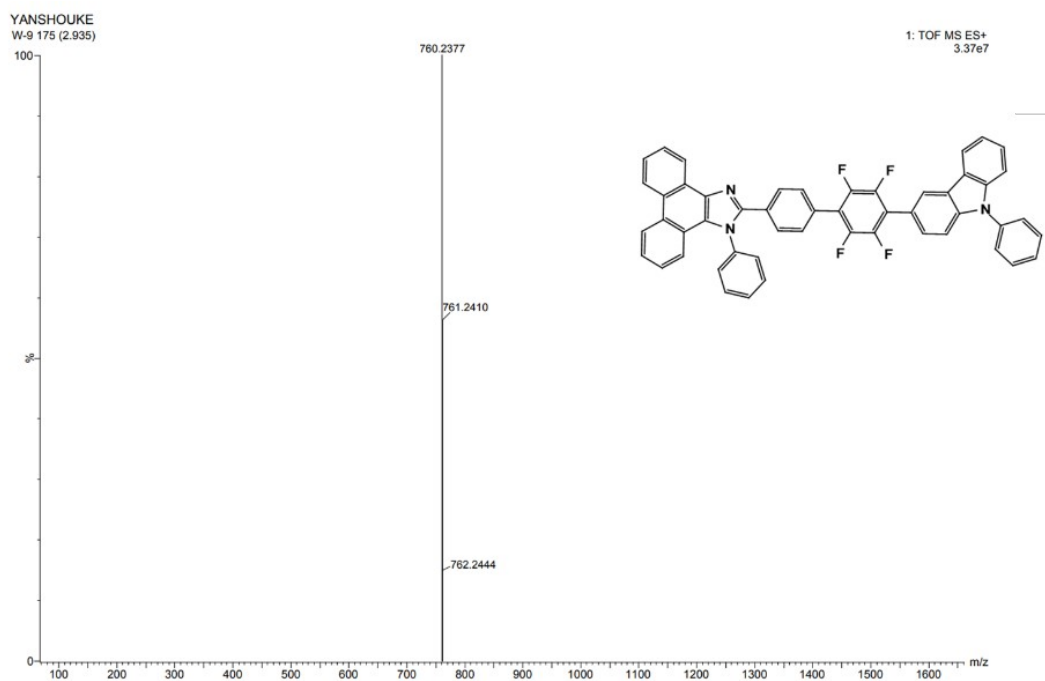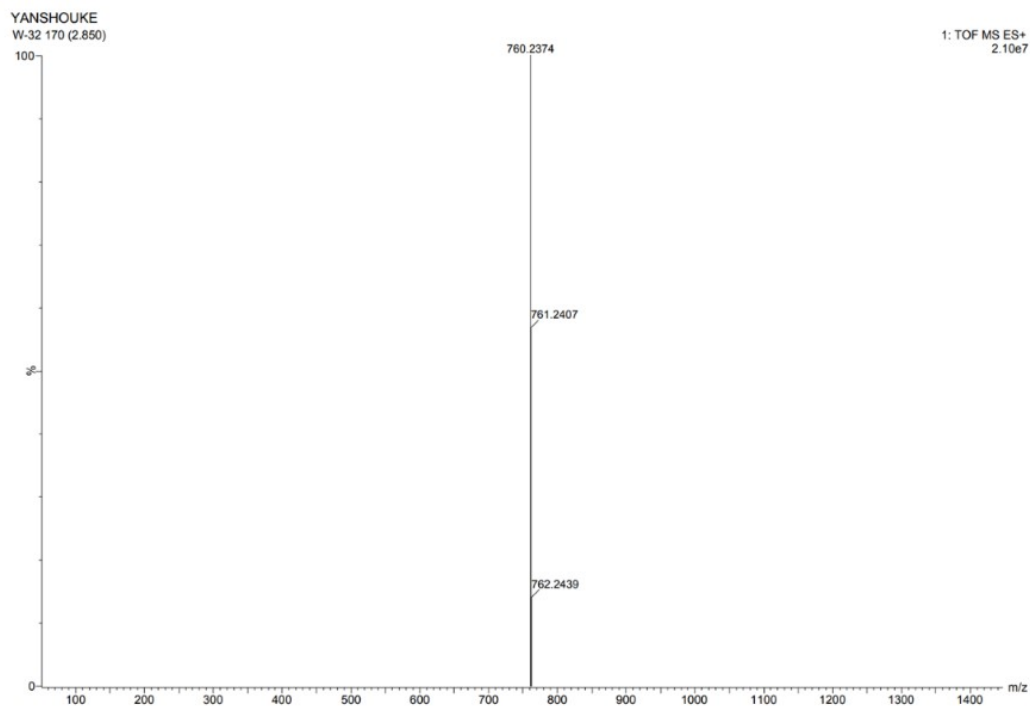**Fig. S17.** The ¹³C NMR spectra of **PICZ4F**.

Fig. S18. The HRMS of **PICZ4F**.

References

[1]   S. Wang, M. Qiao, Z. Ye, D. Dou, M. Chen, Y. Peng, Y. Shi, X. Yang, L. Cui, J. Li, C. Li, B. Wei, W.-Y. Wong, Efficient Deep-Blue Electrofluorescence with an External Quantum Efficiency Beyond 10%, *iScience* **2018**, *9*, 532.

[2]   J. Xin, Z. Li, Y. Liu, D. Liu, F. Zhu, Y. Wang, D. Yan, High-efficiency non-doped deep-blue fluorescent organic light-emitting diodes based on carbazole/phenanthroimidazole derivatives, *J. Mater. Chem. C* **2020**, *8*, 10185.

[3]   C. B. Fialho, T. F. C. Cruz, M. J. Calhorda, L. F. V. Ferreira, P. Pander, F. B. Dias, A. L. Maanita, P. T. Gomes, 9-Borafluoren-9-yl and diphenylboron tetracoordinate complexes of 8-quinolinolato ligands with heavy-atoms substituents: Synthesis, fluorescence and application in OLED devices, *Dyes Pigm*. **2024**, *228*, 112174.

[4]   J. Park, J. Lim, J. H. Lee, B. Jang, J. H. Han, S. S. Yoon, J. Y. Lee, Asymmetric Blue Multiresonance TADF Emitters with a Narrow Emission Band, *ACS Appl. Mater. Interfaces* **2021**, *13*, 45798.

[5]   J. Y. Hu, Y. J. Pu, F. Satoh, S. Kawata, H. Katagiri, H. Sasabe, J. Kido, Bisanthracene-Based

Donor–Acceptor-type Light-Emitting Dopants: Highly Efficient Deep-Blue Emission in Organic Light-Emitting Devices, *Adv. Funct. Mater.* **2014**, *24*, 2064.

[6]   Z. Li, N. Xie, Y. Xu, C. Li, X. Mu, Y. Wang, Fluorine-Substituted Phenanthro[9,10-d]imidazole Derivatives with Optimized Charge-Transfer Characteristics for Efficient Deep-Blue Emitters, *Org. Mater.* **2020**, *2*, 011.

[7]   Y. Zheng, X. Zhu, Z. Ni, X. Wang, Z. Zhong, X. J. Feng, Z. Zhao, Bipolar Molecules with Hybridized Local and Charge-Transfer State for Highly Efficient Deep-Blue Organic Light-Emitting Diodes with EQE of 7.4% and CIEy ∼ 0.05, H. Lu, *Adv. Opt. Mater.* **2021**, *9*, 2100965.

[8]   J. Zhao, B. Liu, Z. Wang, Q. Tong, X. Du, C. Zheng, H. Lin, S. Tao, X. Zhang, EQE Climbing Over 6% at High Brightness of 14350 cd/m2 in Deep-Blue OLEDs Based on Hybridized Local and Charge-Transfer Fluorescence, *ACS Appl. Mater. Interfaces* **2018**, *10*, 9629.

[9]   X. Qiu, S. Ying, C. Wang, M. Hanif, Y. Xu, Y. Li, R. Zhao, D. Hu, D. Ma, Y. Ma, Novel 9,9-dimethylfluorene-bridged D–π–A-type fluorophores with a hybridized local and charge-transfer excited state for deep-blue electroluminescence with CIEy ∼ 0.05, *J. Mater. Chem. C* **2019**, *7*, 592.

[10]   A. Khan, X. Tang, C. Zhong, Q. Wang, S. Y. Yang, F. C. Kong, S. Yuan, A. S. Sandanayaka, C. Adachi, Z. Q. Jiang, L.-L. Liao, Intramolecular-Locked High Efficiency Ultrapure Violet-Blue (CIE-y <0.046) Thermally Activated Delayed Fluorescence Emitters Exhibiting Amplified Spontaneous Emission, *Adv. Funct. Mater.* **2021**, *31*, 2009488.

[11]   I. S. Park, M. Yang, H. Shibata, N. Amanokura, T. Yasuda, Achieving Ultimate Narrowband and Ultrapure Blue Organic Light-Emitting Diodes Based on Polycyclo-Heteraborin Multi-Resonance Delayed-Fluorescence Emitters, *Adv. Mater.* **2022**, *34*, 2107951.

[12]   Y. Yuan, J.-X. Chen, F. Lu, Q.-X. Tong, Q.-D. Yang, H.-W. Mo, T.-W. Ng, F.-L. Wong, Z.-Q. Guo, J. Ye, Z. Chen, X.-H. Zhang, C.-S. Lee, Bipolar Phenanthroimidazole Derivatives Containing Bulky Polyaromatic Hydrocarbons for Nondoped Blue Electroluminescence Devices with High Efficiency and Low Efficiency Roll-Off *Chem. Mater.* **2013**, *25*, 4957.